PLASTIC DEFORMATION OF A POLYGON†

CARL K. YOUNGDAHL
Components Technology Division, Argonne National Laboratory, 9700 South Cass Avenue, Argonne, IL 60439, U.S.A.

Abstract—A closed-form solution is derived for the large plastic deformation of a polygonal frame loaded by a uniform internal pressure. The material of the frame is assumed to be rigid, perfectly plastic, and the effects of large geometric changes are included. A comparison is made between theoretical results and available experimental data for a pressurized hexagonal tube.

INTRODUCTION

Long, thin-walled, polygonal tubes have numerous uses in nuclear reactors and their associated components, such as for fuel subassembly cans, control rod shrouds, instrumentation shrouds, and in-core experiment containments. In addition, polygonal tubes have a potential application as energy-absorbing devices for alleviating severe pressure surges in reactor piping systems.

The purpose of this study is to derive a closed-form solution for the large plastic distortion of a thin-walled polygonal tube subjected to quasi-static internal pressurization, i.e. the loading is slow enough that inertia effects can be neglected. The material of the tube is assumed to be rigid, perfectly plastic. The effect of large geometry changes on redistribution of the loading is included in the analysis. The closed-form solution is useful for providing design estimates for the performance of polygonal tubes subjected to severe loadings and for providing a building block in the development of fluid-structure interaction analyses. It may also be applicable to the validation of finite-element computer programs which have a large displacement, plastic deformation capability.

A comparison of calculated results with experimental data for a pressurized reactor fuel subassembly can is presented, following the derivation of the theoretical solution. Since the subassembly can is made of a material which strain-hardens considerably, the comparison provides a means of evaluating the applicability of the perfect-plasticity assumption.

Finally, an approximate solution, corresponding to a simpler displacement field, is given in the Appendix. The approximate solution gives a good prediction of the deformed shape of the polygon, but violates the yield condition at some points.

STATEMENT OF PROBLEM

Consider a long, thin-walled tube which has a cross section that is a *J*-sided, regular polygon and which is loaded by a uniform internal pressure *P*. The effect of axial variation of the deflection is neglected compared with the large distortion of the cross section, so the problem is equivalent to finding the plastic deformation of a *J*-sided polygonal frame, shown in Fig. 1 for the case *J* = 4. The wall thickness is *H*, the length of a side of the polygon is *L*, and the central angle subtended by a side is 2β. Thus,

$$\beta = \pi/J. \tag{1}$$

The polygonal frame is assumed to be made of a rigid, perfectly plastic material having yield stress σ_y and satisfying the yield condition

$$f(M, N) \equiv \frac{|M|}{M_0} + \frac{N^2}{N_0^2} - 1 \leq 0. \tag{2}$$

† Work performed under the auspices of the U.S. Department of Energy.
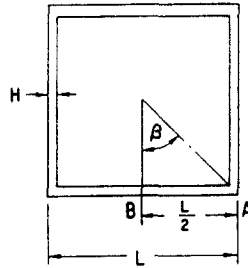
Fig. 1. Polygonal frame, $J = 4$.

Here N and M are, respectively, the resultant membrane force per unit axial length and the bending moment per unit axial length of the original tube; N_0 and M_0 are defined by

$$N_0 = \sigma_y H, \qquad M_0 = \frac{\sigma_y H^2}{4}. \tag{3}$$

The equality in (2) holds at points where plastic hinges form in the deformed polygon, and the inequality holds at points that remain rigid. The plastic flow rule states that, during plastic flow, the generalized strain rate vector has the direction of the exterior normal to the yield surface at the considered generalized stress point[1]. Let ϵ and θ be the stretch and angle change at a plastic hinge; then

$$d\epsilon/d\theta = \frac{\partial f}{\partial N} \Big/ \frac{\partial f}{\partial M}$$

$$= \pm \frac{NH}{2N_0}, \tag{4}$$

where the sign depends on the sign of M.

The polygon remains undeformed for pressures below the yield pressure P_y. At $P = P_y$, plastic hinges develop at the corners and midpoints of the sides. As the pressure is increased above P_y, the corner hinges remain fixed, but each center hinge splits, resulting in two hinges that move outward. Figure 2 shows a typical half-side, with the corner hinge at A and the other hinge having moved from its initial position at B to its final position at $s = \Lambda$, where s is the curvilinear coordinate measured along the side. The half-side is divided into a rotating rigid straight portion and a curved portion that is developed by the moving hinge as the pressure is increased. The hinge conditions are thus

$$f = 0 \text{ at } s = L/2,$$

$$f = 0, \qquad \frac{df}{ds} = 0 \text{ at } s = \Lambda, \tag{5}$$

$$f < 0 \text{ for } 0 \le s < \Lambda \text{ and } \Lambda < s < L/2.$$

Figure 3 is a free-body diagram of an undeformed and deformed half-side. The coordinates ξ, η are measured from the center of the side and define the location of the
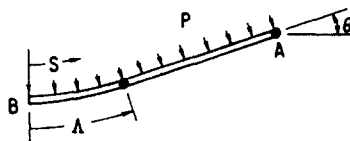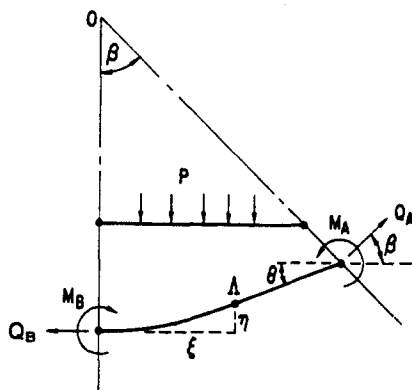

Fig. 2. Half-side of deformed frame.

Fig. 3. Free-body diagram.

hinge at Λ. The symmetry of the polygon requires that the deflection of the corner A and midside B be radial and that the resultant forces Q_A and Q_B be perpendicular to OA and OB, respectively. Therefore,

$$N_A = Q_A \cos(\beta - \theta),$$
$$N_B = Q_B, \tag{6}$$

where θ is the angle of rotation of the straight portion.

The equilibrium equations for the half-side are

$$P\xi + P \left(\frac{\overline{L}}{2} - \Lambda\right) \cos\theta - Q_A \sin\beta = 0,$$

$$-Q_B + P\eta + P \left(\frac{\overline{L}}{2} - \Lambda\right) \sin\theta + Q_A \cos\beta = 0, \tag{7}$$

$$M_B - M_A + Q_B\eta - Q_A \left(\frac{\overline{L}}{2} - \Lambda\right) \sin(\beta - \theta) + \frac{P}{2}\left[\left(\frac{\overline{L}}{2} - \Lambda\right)^2 - \xi^2 - \eta^2\right] = 0.$$

where $\overline{L}$ is the length of the side of the deformed polygon.

In the region $\Lambda \leq s \leq \overline{L}/2$, we have, using eqns (6) and (7),

$$N(s) = P \frac{\cos(\beta - \theta)}{\sin\beta} \left[\xi + \left(\frac{\overline{L}}{2} - \Lambda\right) \cos\theta\right],$$

$$M(s) = P \frac{\sin(\beta - \theta)}{\sin\beta} \left[\xi + \left(\frac{\overline{L}}{2} - \Lambda\right) \cos\theta\right] \tag{8}$$

$$\times \left(\frac{\overline{L}}{2} - s\right) - \frac{P}{2}\left(\frac{\overline{L}}{2} - s\right)^2 + M_A.$$

The difference between the lengths of the deformed and undeformed sides will be neglected in the equilibrium equations in order that a closed-form solution may be obtained. This assumption is reasonable because the results show that the stretch in a side is small compared to its original length. However, the plastic stretch is readily incorporated into the geometric compatibility equations for the deformed shape. Since $N_\Lambda = N_A$, the magnitude of $d\epsilon/d\theta$ is the same at both hinges by eqn (4); since the side is rigid between the hinges, the instantaneous magnitude of the angle change is the same at each of them. Consequently the instantaneous magnitude of $d\epsilon$ is the same at both hinges, and the accumulated stretch in the region swept through by the moving
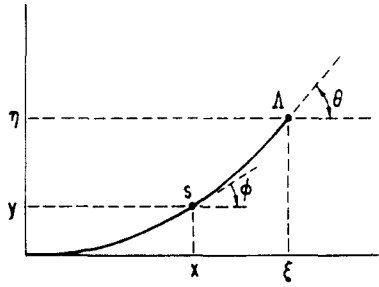
Fig. 4. Nomenclature for curved portion of half-side.

hinge is equal to the total stretch accumulated at the corner. The total stretch Δ of a half-side is thus equal to 2ϵ and is found from eqn (4) to be

$$\Delta = \frac{H}{N_0} \int_0^\theta N_A \, d\theta, \tag{9}$$

where N_A varies as the pressure is increased from P_y to its final value P. If we let δ_A and δ_B denote the outward radial displacement of the corner and midside, geometric compatibility then requires that

$$\delta_A \sin \beta = \left(\frac{L}{2} - \Lambda + \Delta\right) \cos \theta + \xi - \frac{L}{2},$$

$$\delta_B = \delta_A \cos \beta + \left(\frac{L}{2} - \Lambda + \Delta\right) \sin \theta + \eta. \tag{10}$$

Figure 4 shows the curved portion of the side generated as the pressure is increased from P_y to P. At an intermediate pressure the hinge is at point s with coordinates x, y. The slope of the curved side at s is $\tan \phi$. Differential geometry then gives

$$\frac{dx}{d\phi} = \frac{ds}{d\phi} \cos \phi,$$

$$\frac{dy}{d\phi} = \frac{ds}{d\phi} \sin \phi. \tag{11}$$

Since bending occurs only at the hinges, the previously curved part of the side does not change shape as the hinge moves towards its final position Λ. Consequently, determining s and ϕ as functions of intermediate pressure generates the shape of the curved part of the side.

SOLUTION

Using eqns (2) and (8), the hinge condition $df/ds = 0$ at $s = \Lambda$ implies that

$$\xi = \left(\frac{L}{2} - \Lambda\right) \sin \theta \cos(\beta - \theta). \tag{12}$$

From the first of eqns (8), we have

$$N_A = N_\Lambda = P\left(\frac{L}{2} - \Lambda\right) \cot(\beta - \theta). \tag{13}$$

Since $f = 0$ at both $s = 0$ and $s = \Lambda$ and since $N_A = N_\Lambda$, then $|M_A| = |M_\Lambda|$ and the second part of eqn (8) gives

$$M_\Lambda = -M_A = \frac{P}{4}\left(\frac{L}{2} - \Lambda\right)^2.$$ (14)

The yield condition at a hinge therefore implies

$$\frac{P}{\sigma_y}\left[\frac{P}{\sigma_y}\cot^2(\beta - \theta) + 1\right]\left(\frac{L}{2} - \Lambda\right)^2 - H^2 = 0.$$ (15)

It is more convenient to consider θ to be the independent variable rather than P. Consequently, eqn (15) is solved for P to give

$$\frac{P}{\sigma_y} = \frac{8\left(\dfrac{H}{L - 2\lambda}\right)^2}{1 + \left\{1 + 16\left[\dfrac{H\cot(\beta - \theta)}{L - 2\Lambda}\right]^2\right\}^{1/2}}.$$ (16)

At the yield pressure P_y, both θ and Λ are zero. Therefore, P_y for a J-sided polygon is

$$\frac{P_y(J)}{\sigma_y} = \frac{8H^2}{L^2 + L(L^2 + 16H^2\cot^2\beta)^{1/2}}.$$ (17)

Consider an equivalent circular ring which has the same wall thickness and perimeter as the polygonal frame; let its radius be R_0 and its yield pressure be P_{y0}. Using (1),

$$R_0 = \frac{JL}{2\pi} = \frac{L}{2\beta}$$ (18)

and

$$P_{y0} = \frac{H\sigma_Y}{R_0}.$$ (19)

From eqns (17) and (19),

$$P_{y0} = \operatorname*{Lim}_{J\to\infty} P_y(J).$$ (20)

The hinge location Λ remains to be determined as a function of θ. The relationship (12) between ξ, Λ, and θ holds between x, s, and ϕ (Fig. 4) at a lower pressure; i.e.

$$x = \left(\frac{L}{2} - s\right)\sin\phi\cot(\beta - \phi).$$ (21)

Substitution into the first of eqns (11) and integration over the whole curve then gives

$$\int_0^\Lambda \frac{ds}{\dfrac{L}{2} - s} = \frac{1}{\sin\beta}\int_0^\theta\left[\cos\phi\cos(\beta - \phi) + \frac{\sin\phi}{\sin(\beta - \theta)}\right]d\phi.$$ (22)

The solution of eqn (22) for Λ as a function of θ is

$$\Lambda = \frac{L}{2}\left[1 - \frac{\sin(\beta - \theta)}{\sin\beta}e^{-G(\theta)}\right], \tag{23}$$

where

$$G(\theta) \equiv \frac{\sin\theta\cos(\beta - \theta) - \theta\cos\beta}{2\sin\beta}. \tag{24}$$

The substitution of eqn (23) into eqn (16) gives P as a function of θ,

$$P(\theta) = \frac{8\sigma_y H^2\sin^2\beta\, e^{-2G(\theta)}}{L^2\sin^2(\beta - \theta) + L[L^2\sin^4(\beta - \theta) + 16H^2\sin^2\beta\cos^2(\beta - \theta)\,e^{2G(\theta)}]^{1/2}}. \tag{25}$$

To complete the solution, we use eqns (9), (11), (12) and (23) to obtain ξ, η and Δ as functions of θ:

$$\xi = \frac{L\sin\theta\cos(\beta - \theta)}{2\sin\beta}e^{-G(\theta)},$$

$$\eta = \frac{L}{2\sin^2\beta}\int_0^\theta[\sin(\beta - \phi)\cos(\beta - \phi)\cos\phi + \sin\phi]\sin\phi\, e^{-G(\phi)}\,d\phi, \tag{26}$$

$$\Delta = \frac{L}{2\sigma_y\sin\beta}\int_0^\theta P(\phi)\cos(\beta - \phi)\,e^{-G(\phi)}\,d\phi.$$

The corner and midside displacements can then be calculated from eqn (10).
The membrane forces and bending moments at the hinges and midside are

$$N_\Lambda(\theta) = N_A(\theta) = \frac{P(\theta)L\cos(\beta - \theta)}{2\sin\beta}e^{-G(\theta)},$$

$$M_\Lambda(\theta) = -M_A(\theta) = \frac{P(\theta)}{16}\left[\frac{L\sin(\beta - \theta)}{\sin\beta}e^{-G(\theta)}\right]^2, \tag{27}$$

$$N_B(\theta) = \frac{N_\Lambda(\theta)}{\cos\theta} + P(\theta)[\eta(\theta) - \xi(\theta)\tan\theta],$$

$$M_B(\theta) = M_\Lambda(\theta) - N_B(\theta)\eta(\theta) + \tfrac{1}{2}P(\theta)[\xi^2(\theta) + \eta^2(\theta)].$$

The force and moment distributions for $0 \leq s \leq \Lambda$, i.e. $0 \leq \phi \leq \theta$, are

$$N(\theta, s) = N_B(\theta)\cos\phi + P(\theta)[x(\phi)\sin\phi - y(\phi)\cos\phi], \tag{28}$$

$$M(\theta, s) = M_B(\theta) + N_B(\theta)y(\phi) - \tfrac{1}{2}P(\theta)[x^2(\phi) + y^2(\phi)]$$

where s, x and y are related to ϕ as Λ, ξ and η are related to θ [see eqns (23) and (26)]. The distributions for $\Lambda \leq s \leq L/2$ are

$$N(\theta, s) = N_\Lambda(\theta), \tag{29}$$

$$M(\theta, s) = M_\Lambda - \tfrac{1}{2}P(\theta)[s - \Lambda(\theta)]^2.$$

As θ increases, M_B decreases and eventually changes sign. If the expressions for N_B and M_B are substituted into eqn (2), a value of θ, denoted by θ_m, can be determined

which satisfies the yield condition. A new hinge then forms at the midside. For $P >$ P_m, where $P_m = P(\theta_m)$, this new hinge also moves along the previously deformed side, and the solution derived in this section is no longer valid. However, the results in the next section will show that Λ is close to the corner and the polygon is nearly circular at $P = P_m$.

RESULTS

Results are shown in this section for $R_0/H = 20$, which, from eqn (19), corresponds to

$$\frac{L}{H} = \frac{40\pi}{J}. \tag{30}$$

In Fig. 5, θ is drawn as a function of P/P_{y0} for various polygonal frames, as computed from eqn (25). The circled points correspond to P_m, and the dashed portions of the curves are the approximate solution discussed in the Appendix. Near $P = P_y$, the angular deformation changes rapidly for small increases in P if J is small, but for larger
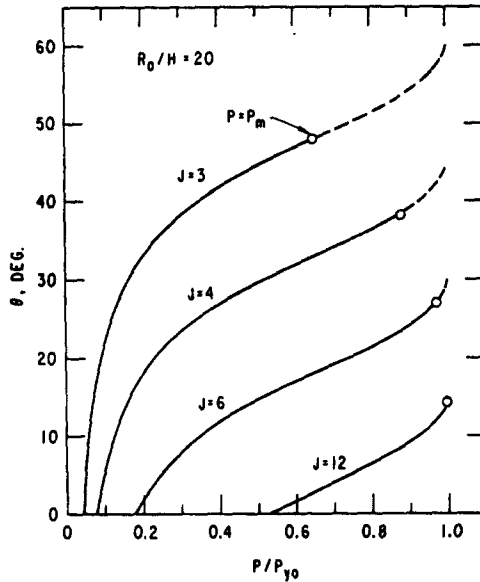

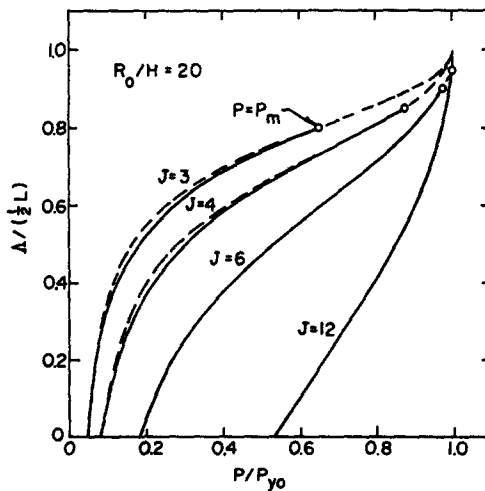Fig. 5. Angle θ as a function of pressure for J-sided polygons.

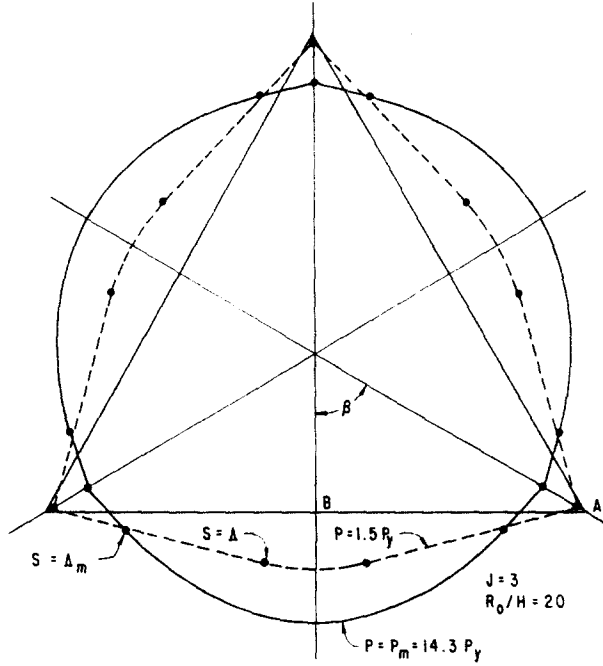Fig. 6. Hinge location Λ as a function of pressure for J-sided polygons.

Fig. 7. Deformed triangular frame for $P = 1.5\ P_y$ and $P = P_m = 14.3\ P_y$.

J more of the load is balanced by the membrane force. Since Λ is known as a function of θ, eqn (23) can be combined with the above result to give hinge location as a function of pressure, as shown in Fig. 6.

Figure 7 shows the deformed shape of a triangular frame for $P = 1.5\ P_y$ and $P = P_m = 14.3\ P_y$. The moving hinges are near the corners for the larger load and the
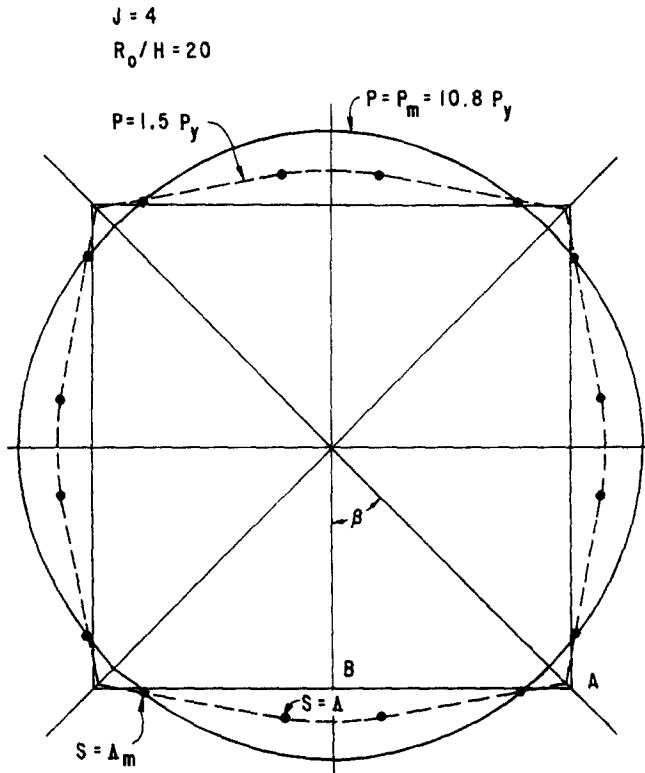
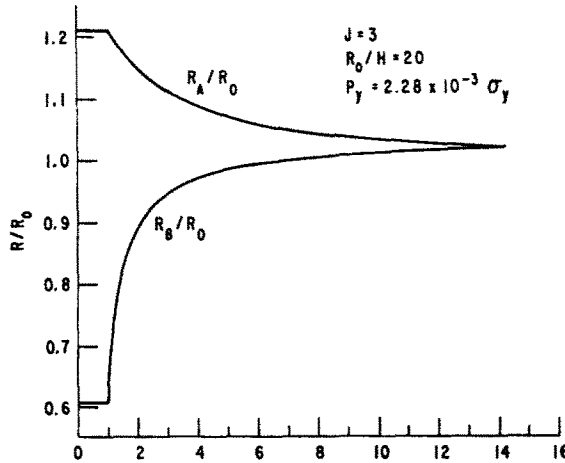Fig. 8. Deformed square frame for $P = 1.5\ P_y$ and $P = P_m = 10.8\ P_y$.

Fig. 9. Corner and midside locations as functions of pressure for triangular frame.
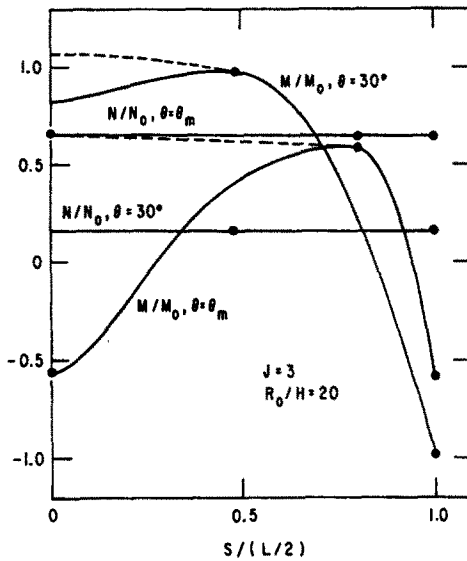

Fig. 10. Bending moment and membrane force distribution in triangular frame for $\theta = 30°$ and $\theta = \theta_m = 47.96°$.

deformed shape is nearly circular. The deformation of a square frame is shown in Fig. 8.

The radial locations of the corner and midside of the triangular frame are plotted in Fig. 9 as a function of P/P_y. We see that as P increases both radii approach a value just slightly larger than R_0 because of the small stretch in the side (about 0.7% at P_m).

Figure 10 shows the bending moment and membrane force distribution in the half-side of a triangular frame when $\theta = 30°$ and when $\theta = \theta_m = 47.96°$. The dots indicate the locations of the hinges, and the dashed curves are for the approximate solution presented in the Appendix. Although N varies monotonically for s between 0 and Λ, the variation is so small as to be unnoticeable. In particular, $N_B = 0.1562$ and $N_\Lambda = 0.1544$ for $\theta = 30°$, and $N_B = 0.6604$ and $N_\Lambda = 0.6461$ for $\theta = \theta_m$. Consistent with eqns (5), the magnitude of M is a maximum at Λ and $L/2$ and has zero slope at the moving hinge. A new hinge is just beginning to form at $s = 0$ for $\theta = \theta_m$.

Figure 11 shows the yield condition and f at both the midside and the moving hinge for $P = kP_y$, with $k = 1, 2, \ldots 13, 14.3$; f_Λ is the mirror image of f_Λ in the N axis and moves along the yield curve as P increases. (The triangles belong to the approximate
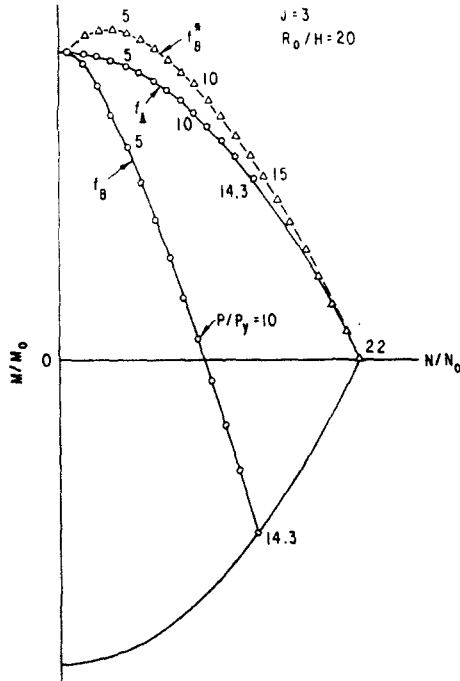
Fig. 11. Yield function $f(M, N)$ at hinge and corner for triangular frame.

solution discussed later.) We see that the midside is rigid for $P > P_y$ until a new hinge with opposite sign forms there at $P = 14.3\, P_y = P_m$.

COMPARISON WITH EXPERIMENT

SRI International pressurized reactor subassembly cans made of several compositions of stainless steel[2]. The cans are long, thin-walled tubes with hexagonal cross
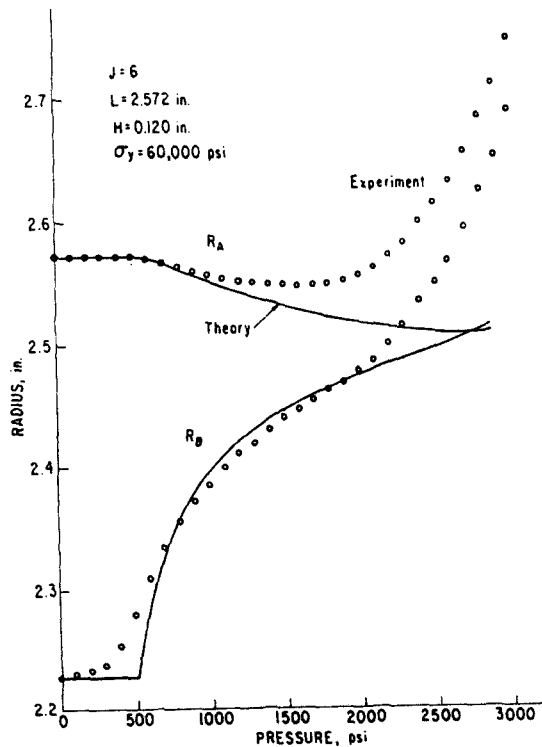

Fig. 12. Comparison of theoretical and experimental deformation of hexagonal tube.

sections and so satisfy the geometrical assumptions of this article. However, stainless steel significantly strain hardens, and the assumption here of perfect plasticity, therefore, is not realistic for the can material. From the range of measured strains in the subassembly cans, a value of σ_y = 60,000 psi would appear to be a reasonable value of yield stress for an equivalent perfectly plastic material to model the stainless steel used in the experiment discussed here. Figure 12 shows changes in radius with pressure at the corners and midside for both the theoretical solution and one of the experiments. The stainless steel does not have a distinct yield point and so the measured deformation at B changes less abruptly at low pressures than the theory predicts. Strain hardening spreads the plastic hinges into plastic zones, so less angle change at the corners would be expected in the experiment. Because the corners then do not pull in as much, more of the load is equilibrated by the membrane force and more stretching of the sides occurs at high pressures. The agreement at high pressures would likely be better if the tube were made of a material with less strain hardening, such as mild steel.

REFERENCES

1. W. Prager, *An Introduction to Plasticity*. Addison-Wesley, Reading, Mass. (1959).
2. D. J. Cagliostro and C. M. Romander, *Experiments on the Response of Hexagonal Subassembly Ducts to Radial Loads*. SRI Project PYD-1960, Third Interim Report, December (1975).

APPENDIX

The curved part of the deformed polygonal frame is very close to a circular arc with radius R_0. Assuming this is the exact deflection shape gives a somewhat simpler solution than obtained previously, which may be more convenient for incorporation into complex analyses such as for fluid-structure interaction. However, the approximate solution violates the yield condition on part of the side of the polygon.

Denoting the approximate solution by asterisked variables, we will put

$$\Lambda^* = R_0\theta = \frac{L\theta}{2\beta},$$

$$\xi^* = \frac{L}{2\beta}\sin\theta, \tag{31}$$

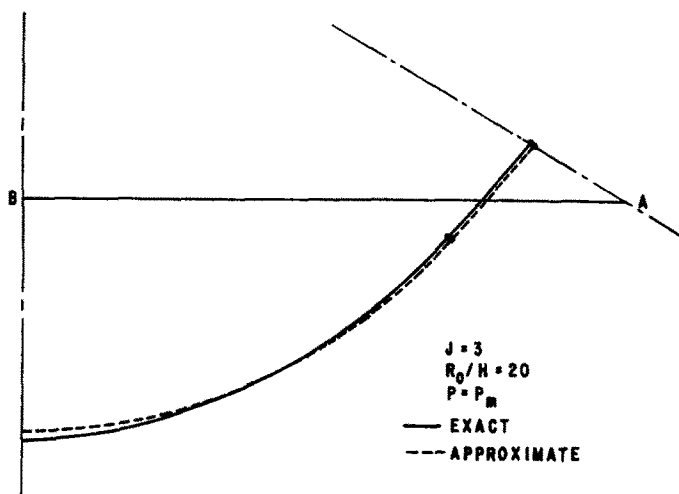$$\eta^* = \frac{L}{2\beta}(1 - \cos\theta).$$

Fig. 13. Deformed half-side of triangular frame for approximate and exact solutions.

Substitution into eqns (5-8) then gives

$$P^*(\theta) = \frac{8\sigma_y H^2 \beta^2 \sin\beta}{L^2 F_1 + L[L^2 F_1^2 + 16H^2\beta^2 F_2]^{1/2}}, \tag{32}$$

where

$$
\begin{aligned}
F_1 &\equiv 2(\beta - \theta)\sin\theta\sin(\beta - \theta) + (\beta - \theta)^2\sin(\beta - 2\theta), \\
F_2 &\equiv \cos^2(\beta - \theta)[\sin\theta + (\beta - \theta)\cos\theta]^2.
\end{aligned}
\tag{33}
$$

The plot of eqn (32) is indistinguishable from that of eqn (25) in Fig. 5 and can be extended on to $\theta = \beta$ when the moving hinge approaches the corner.

Figure 13 shows a comparison between the approximate and exact deflection shapes for the half-side of the triangular frame with $P = P^* = 14.3\, P_y$. It is apparent that the exact shape is very close to a circular arc. However, as evidenced in Figs. 10 and 11, the approximate solution, denoted by the dashed lines, violates the yield condition in the deformed segment.

Consequently, the approximate solution gives a good estimate of the variations of the deflection shape and membrane force with pressure, but is considerably in error in predicting the bending moment distribution and violates the yield condition.